Proposal for a long-lived quantum memory using matter-wave optics with Bose-Einstein condensates in microgravity

Elisa Da Ros,[1,*] Simon Kanthak,[1,*] Erhan Sağlamyürek,[2,3,†] Mustafa Gündoğan,[1,‡] and Markus Krutzik[1,4,§]

[1]*Institut für Physik and IRIS Adlershof, Humboldt-Universität zu Berlin, Newtonstraße 15, 12489 Berlin, Germany*

[2]*Department of Physics and Astronomy, University of Calgary, Calgary, Alberta, Canada T2N 1N4*

[3]*Department of Physics, University of Alberta, Edmonton, Alberta, Canada T6G 2E1*

[4]*Ferdinand-Braun-Institut (FBH), Gustav-Kirchoff-Straße 4, 12489 Berlin, Germany*

(Received 21 December 2022; accepted 24 April 2023; published 5 July 2023)

Bose-Einstein condensates are a promising platform for optical quantum memories but suffer from several decoherence mechanisms, leading to short memory lifetimes. While some of these decoherence effects can be mitigated by conventional methods, density-dependent atom-atom collisions ultimately set the upper limit of the quantum memory lifetime to timescales of seconds in trapped Bose-Einstein condensates. We propose a quantum memory technique that utilizes microgravity as a resource to minimize such density-dependent effects. We show that by using optical atom lenses to collimate and refocus the freely expanding atomic ensembles, in a semi-ideal environment, the expected memory lifetime is only limited by the quality of the background vacuum. We anticipate that this method can be experimentally demonstrated in Earth-bound microgravity platforms or space missions, eventually leading to storage times of minutes and unprecedented time-bandwidth products of 10^{10}.

DOI: 10.1103/PhysRevResearch.5.033003

I. INTRODUCTION

Optical quantum memories (QMs) are devices that can faithfully and reversibly store and recall the quantum states of light. They are required in many applications in quantum information science such as long-distance quantum communications [1,2], deterministic generation of multiphoton states [3], and quantum computation [4]. A recent idea is to deploy QMs in space in order to enable globe-spanning quantum networks [5–8], ultralong-baseline Bell experiments [9–12], and probing the interplay between gravity and quantum physics [13] for which a storage time τ_{mem} of around $\sim$1 s is needed. Several systems have been proven useful for such reversible mapping between light and matter qubits. These include solid-state [14–19] and atomic systems [20–33]. Among these, cold-atomic gases have recently been deployed in space for a number of experiments: optical atomic clocks [34] and the first Bose-Einstein condensate (BEC) on board a sounding rocket [35] and the International Space Station (ISS) [36]. In addition to these, new space missions using cold atoms are being envisioned [37–39] and currently in development [40,41]. Cold-atom-based QMs would share the same technical infrastructure with these experiments.

A BEC platform has unique advantages over cold atoms (obeying a thermal distribution) for optical QMs due to the inhibition of thermal motion (allowing a long memory lifetime) and its high atomic density (leading to efficient operation). However, condensates are still affected by several decoherence mechanisms. Among these, decoherence due to magnetic field inhomogeneities [29,33] can be mitigated by employing rephasing protocols based on dynamical decoupling [42], and those caused by AC-Stark shifts that are due to inhomogeneous optical trapping beams can be prevented by employing magic wavelength techniques [43,44]. On the other hand, losses due to atom-atom collisions are usually not reversible, and cannot be mitigated by such measures. The collisions of cold atoms with the background gas (i.e., one-body collisions) can be controlled only with the vacuum quality, while the collision rates between two or three atoms within the cold ensemble (i.e., two-body and three-body collisions) increase with increasing atom density. These processes become relevant beyond storage times of $\sim$1 ms. However, a maximum storage time of around $\sim$1 s has been observed with bright pulses in a sodium BEC by tuning the atom-atom collision cross sections via external magnetic fields [45].

In this paper, we propose a quantum storage scheme that exploits matter-wave optics to tune the density of the atomic ensemble to minimize the effects of density-dependent collisions. This is achieved by letting the condensate expand after writing the quantum state of incoming photons into an internal state of the atoms in the condensate, which is followed by

*These authors contributed equally to this work.

†Present address: Lawrence Berkeley National Laboratory and Department of Physics, University of California, Berkeley, California, 94720, USA.

‡mustafa.guendogan@physik.hu-berlin.de

§markus.krutzik@physik.hu-berlin.de

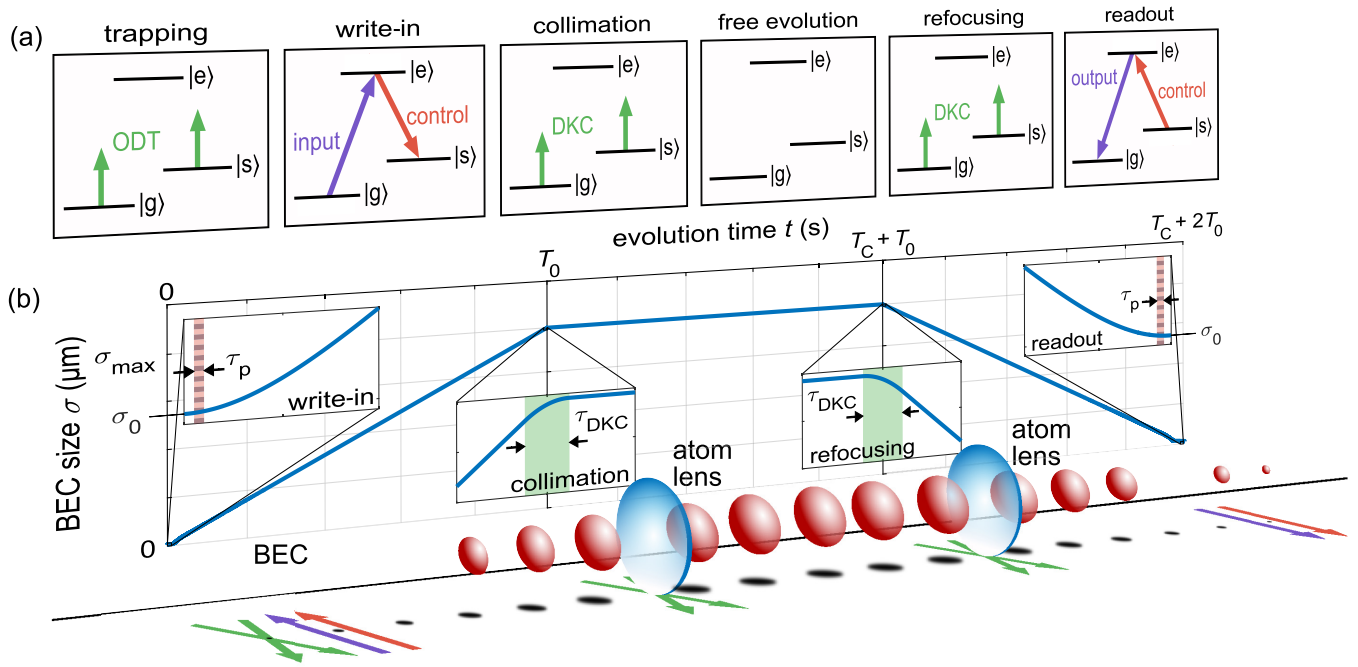

FIG. 1. Protocol for a long-lived quantum memory utilizing interaction-driven expansion and delta kick collimation (DKC) of a Bose-Einstein condensate (BEC) in microgravity. (a) Λ-type three-level structure together with the light fields employed during (b) different stages of the size evolution of the BEC. The quantum state of single-photon pulses is imprinted into an internal excitation of a BEC shortly after its release from an optical dipole trap (ODT). Brief exposure of the BEC to two consecutive optical lensing potentials allows us to stop and subsequently reverse the interaction-driven expansion via DKC. This protocol allows for transition between the complementary density regimes needed for an efficient write-in and readout of the memory at high optical depths (ODs) and large coherence times for long-time storage at low atomic densities, respectively.

employing the delta kick collimation (DKC) technique [46–49], first to collimate and then to refocus the BEC for efficient readout of the stored excitation. This protocol is carried out in a microgravity environment, which prevents the fall of the center of mass without the need for any type of inhomogeneous field to levitate the atoms. We show that this technique would allow storage times that are orders of magnitude beyond what is possible in ground-based experiments and, in fact, only limited by the quality of the background vacuum. We expect our protocol to reach a few minutes of storage time with the state-of-the-art background vacuum values [50,51].

II. STORAGE AND RETRIEVAL PROTOCOL

We assume a pure BEC initially trapped in an optical dipole trap (ODT), as illustrated in Fig. 1. To circumvent decoherence due to AC-Stark shifts, the quantum state of single-photon pulses is imprinted within the BEC only shortly after its release from the trap. The timing of the write pulse is set to mode-match the light intensity and atomic density distributions with negligible reduction in optical depth (OD). During free expansion, the internal energy is converted into kinetic energy, yielding a reduction in the density and therefore in the two-body collisions. After a set time T_0, the BEC is exposed to a tailored, optical potential for a short duration of τ_{DKC}. This delta kick acts as an optical atom lens [48,52–54], resulting in a narrow momentum distribution. After a chosen collimation time T_{C}, a second DKC pulse is applied to refocus the ensemble. At this point ($T_{\mathrm{C}} + 2\,T_0$), it is possible to faithfully recall the stored quantum information at the original higher OD. Our protocol thus allows transitioning between the complementary density regimes needed for an efficient write-in and readout at high ODs and coherent storage in a dilute quantum gas. This is achieved by exploiting the mean-field driven expansion of a self-interacting BEC which is nearly stopped and reversed via DKC.

The quantum memory itself is based on a Λ-type three-level system as represented in Fig. 1. The states $|g\rangle$ and $|s\rangle$ represent the ground states of the hyperfine structure of the ^{87}Rb D_1 line, $|5^2S_{1/2}, F = 1\rangle$ and $|5^2S_{1/2}, F = 2\rangle$, respectively, while $|e\rangle$ is the excited state $|5^2P_{1/2}, F = 1\rangle$. Collinear probe and control beams address the $|g\rangle \longleftrightarrow |e\rangle$ and $|s\rangle \longleftrightarrow |e\rangle$ transitions, respectively. The use of collinear beams [55] ensures both the optimal spin storage and phase-matching condition, which eliminates decoherence due to recoil collisions [33].

Although ensemble-based memories generally follow similar considerations [56], we choose to incorporate the Autler-Townes splitting (ATS) method [33,57] into our approach as it requires lower OD and control power for efficient storage of broadband pulses compared with other memory protocols implemented in cold-atom systems, such as electromagnetically induced transparency [58], which makes it more attractive for applications in quantum information science. Furthermore, lower requisites on these properties make the ATS protocol

more robust against four-wave mixing noise [33], which is another important feature for practical applications. We further note that the applied DKC pulses, being far off-resonant, do not optically pump the atoms to generate fluorescence and four-wave mixing noise, thereby ensuring operation in the single-photon regime.

III. BEC EXPANSION AND COMPRESSION DYNAMICS

We predict the dynamics of the BEC through a variational ansatz to numerically solve the time-dependent Gross-Pitaevskii equation

$$i\hbar\frac{\partial}{\partial t}\psi(\vec{r},t) = \left[-\frac{\hbar^2}{2m}\nabla^2 + V_{\mathrm{DKC}}(\vec{r},t) + U_0\rho(\vec{r},t)\right]\psi(\vec{r},t) \tag{1}$$

following a scaling approach [59,60], where $V_{\mathrm{DKC}}(\vec{r},t)$ represents the lensing potential and $U_0 = 4\pi\hbar^2\mathrm{Re}(a_{\mathrm{sc}})N_0/m$ characterizes the interaction and is defined by the real part of the s-wave scattering length a_{sc} [61] for a ground-state BEC with N_0 atoms of mass m.

As trial functions, we simply utilize a Gaussian-shaped atomic wave function $\psi(\vec{r},t)$ with corresponding spatial density distribution $\rho(t)$ expressed as

$$\rho(t) = |\psi(t)|^2 = \underbrace{\frac{N_0}{(2\pi)^3}\prod_{\xi\in\{x,y,z\}}\sigma_\xi^{-1}(t)}_{=\rho_0(t)}\exp\left(-\frac{\xi^2}{2\sigma_\xi^2(t)}\right), \tag{2}$$

where $\rho_0(t)$ represents the peak density. The standard deviation $\sigma_\xi(t)$ of the atomic density can be related to the Thomas-Fermi radius $\sigma_\xi = R_\xi/\sqrt{7}$, knowing the parabolic shape of a BEC [62].

The lensing potential is well described by the harmonic approximation $V_{\mathrm{DKC}}(\vec{r},t) = 1/2m\sum_\xi \omega_\xi^2\xi^2$ if the BEC is located close to the center of the optical trap and if the characteristic size of the generating beams is $w_0 \gg \sigma_\xi$. Any anharmonicity of the potential would cause lens aberrations and will ultimately limit the achievable storage times and efficiency of the information readout due to the attainable collimation times [49] and minimum sizes during refocusing [48], respectively.

For our study, we initialize an isotropic BEC of size $\sigma_0 = 3\,\mu\mathrm{m}$ with $N_0 = 1\times10^5$ ^{87}Rb atoms. After $T_0 = 1\,\mathrm{s}$ of free expansion, we apply a DKC potential with trap frequency $\omega = 2\pi\times 2.25\,\mathrm{Hz}$ for a symmetrically centered box pulse of duration $\tau_{\mathrm{DKC}} = 5\,\mathrm{ms}$. After further evolution for T_{C}, the BEC is exposed again to the same DKC potential. Further details are provided in Appendix A. The trap frequency is chosen to mode-match the final and initial wave functions. The total storage time, τ_{mem}, of the memory in this protocol is then $\approx T_{\mathrm{C}} + 2\,T_0$.

In general, illumination of the ensemble with an inhomogeneous light field, as needed for optical DKC, can affect the system coherence. Assuming a crossed-beam ODT at 1064 nm as the origin of the lensing potential, we calculate the differential AC-Stark shift of the two ground states of ^{87}Rb to be $\delta\nu_{\mathrm{AC}} \ll \tau_{\mathrm{DKC}}^{-1}$, granting a negligible decoherence during the DKC pulses; see Appendix B.

IV. EFFICIENCY CALCULATIONS WITH DENSITY ENGINEERED ENSEMBLE

Assuming that the untrapped ensemble is shielded from any magnetic field inhomogeneities, the overall efficiency of photon retrieval can then be expressed as a function of the atomic density distribution and peak density as

$$\eta_{\mathrm{tot}}(t) = \eta_{\mathrm{DKC}}^2\cdot\eta_1(t)\cdot\eta_2(\rho_0(t))\cdot\eta_{\mathrm{ATS}}(\rho(t)), \tag{3}$$

where η_{DKC} indicates the efficiency of the DKC procedure, $\eta_1(t)$ and $\eta_2(\rho_0(t))$ are associated with the one-body and two-body collisions, respectively, and, finally, the factor $\eta_{\mathrm{ATS}}(\rho(t))$ represents the combined efficiencies of the ATS write-in and readout steps.

For the purpose of this work, η_{DKC} is set to 1. This corresponds to the assumption of ideal harmonic potentials for the implementation of the DKC procedures and thus neglects possible lens aberrations that would affect the atom distribution [48]. This ideal case might be accomplished in experiments utilizing time-averaged optical potentials [63].

The efficiency associated with the atom losses due to the collisions with the background gas within the vacuum chamber, $\eta_1(t)$, follows an exponential decay. In Ref. [51], Nirrengarten *et al.* achieve a lifetime of about 115 s associated with a background pressure of 3×10^{-11} mbar. We set this value as the one-body collision lifetime τ_1 used in this paper. The term $\eta_2(\rho_0(t))$ expresses the exponential decay of the memory efficiency due to two-body collisions between cold Rb atoms. For the states and densities taken into account in this paper, the contribution of the three-body collisions is negligible compared with the other collisional losses [64].

Figure 2(a) shows a comparison of the time evolution of the condensate size for two different collimation times (blue and orange lines), along with the scenario in which the BEC is not released from the trap at all (yellow line). The color code is the same for the other panels in the figure. In both expanding cases, the condensate peak density drops from its initial value $\rho_0(0) = 2.3\times10^{14}\,\mathrm{cm}^{-3}$ to $\rho_0(T_0 = 1\,\mathrm{s}) = 7\times10^6\,\mathrm{cm}^{-3}$ at the time of the first DKC pulse. After a duration of $T_{\mathrm{C}} = 3\,\mathrm{s}$ (blue) or $T_{\mathrm{C}} = 98\,\mathrm{s}$ (orange), the second DKC pulse is applied, which causes the BEC to refocus and reach its minimum size again at $\tau_{\mathrm{mem}} \approx T_{\mathrm{C}} + 2\,T_0$, when the memory is read out. The corresponding τ_{mem} are $\approx$5 s (blue) or $\approx$100 s (orange). The inset shows the detailed evolution of the BEC size around the focus for the case with $T_{\mathrm{C}} = 3\,\mathrm{s}$.

The time evolutions of peak density corresponding to the simulated sizes in Fig. 2(a) allow us to calculate the time-dependent two-body collisions decay rate, $\gamma_{2\text{-body}}(t)$, as [33,65]

$$\gamma_{2\text{-body}}(t) = \frac{4h\,\mathrm{Im}(a_{\mathrm{sc}})\rho_0(t)}{m}, \tag{4}$$

where $\mathrm{Im}(a_{\mathrm{sc}})$ is the imaginary part of the s-wave scattering length. Figure 2(b) shows a reduction of more than seven orders of magnitude in the two-body decay rate during T_0, compared with the trapped case with constant peak density. The inset highlights again the behavior around the focus for the case with $T_{\mathrm{C}} = 3\,\mathrm{s}$.

With this time-dependent decay rate, the intrinsic efficiency due to two-body collisions is found upon integration

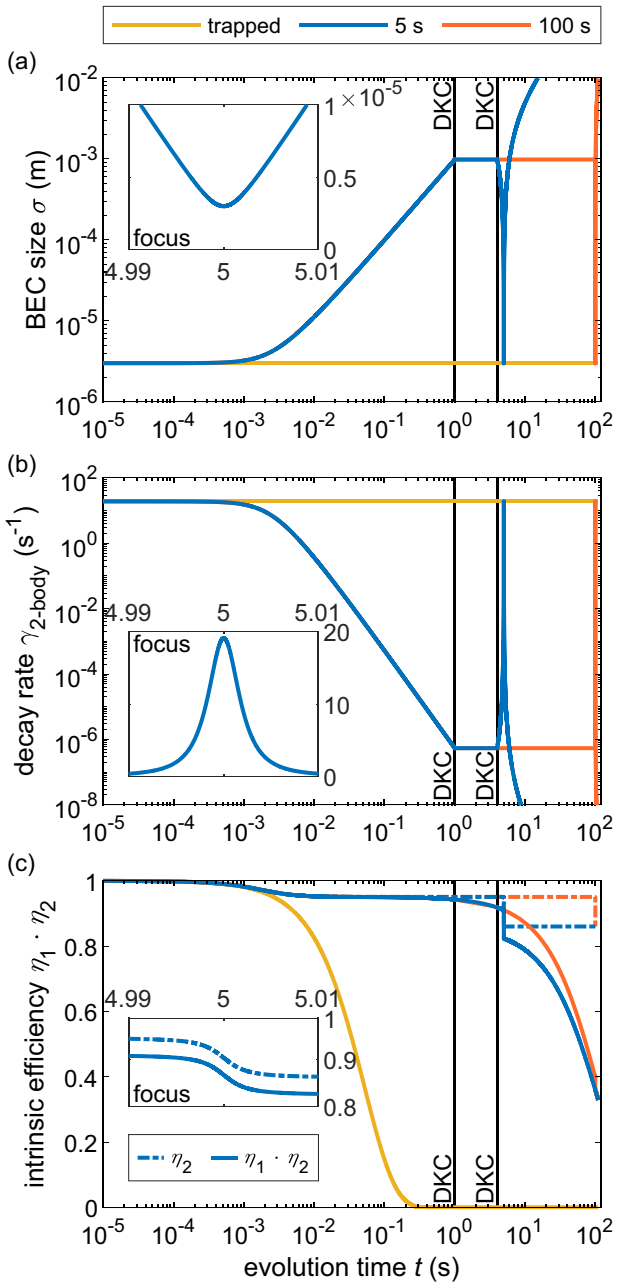

FIG. 2. BEC dynamics and intrinsic memory efficiency. Time evolution of (a) the BEC size σ and (b) the corresponding decay rates $\gamma_{2\text{-body}}$ and its effect on (c) the intrinsic memory efficiency (i.e., not including write-in and readout efficiencies) due to only two-body collisions (dashed lines) and a combination of two- and one-body collisions (solid lines). We compare our protocol with storage times $\tau_{\text{mem}} \approx 5\,\text{s}$ (blue) and $\tau_{\text{mem}} \approx 100\,\text{s}$ (orange) together with the trapped case (yellow). The insets show a zoom of the respective changes during the focus of the BEC for the case $\tau_{\text{mem}} \approx 5\,\text{s}$, in linear scaling. The black vertical lines indicate the timing of the DKC pulses for the case with $\tau_{\text{mem}} \approx 5\,\text{s}$. See Appendix A for simulation details.

over time as

$$\eta_2(\rho_0(t)) = \exp\left(-\int_0^t \frac{\rho_0(t')}{\kappa} dt'\right), \tag{5}$$

where $\kappa = m/(4h\,\text{Im}(a_{\text{sc}}))$.

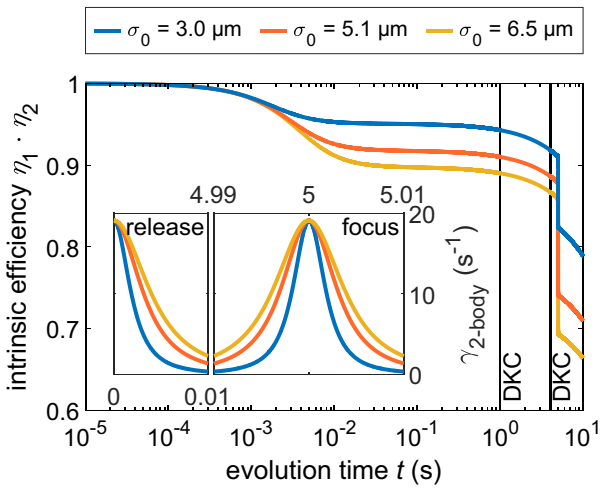

FIG. 3. Intrinsic memory efficiency for different initial BEC sizes σ_0 and common initial peak density $\rho_0(0) = 2.3 \times 10^{14}\,\text{cm}^{-3}$. The black lines indicate the timing of the DKC pulses to collimate and refocus the BEC. The inset shows the evolution of the two-body decay rate shortly after release and during refocusing, in linear scaling. See Appendix A for simulation details.

The intrinsic memory efficiency, $\eta_1(t) \cdot \eta_2(\rho_0(t))$, is plotted in Fig. 2(c). The solid lines include the effects of one- and two-body collisions, whereas the dashed lines show only the effects of two-body collisions. It is evident from the figure that the constant high density of the trapped case yields a lifetime limit of around 100 ms by two-body collisions. In contrast, the lifetime can be extended for the expanding and refocused cases, proving that the memory decay rate can be tuned by varying the BEC density via our protocol. The spike in $\gamma_{2\text{-body}}$ [see Fig. 2(b)], due to the increased density during refocusing, results in a sudden drop in intrinsic efficiency (from 0.92 to 0.83), as seen in the inset of Fig. 2(c). The magnitude of the drop depends on the initial atom distribution, as shown in the following paragraph. The inset focuses on the comparison between the effects of one- and two-body collisions, $\eta_1 \cdot \eta_2$, and the single two-body contribution, η_2, around the focus, for the case $\tau_{\text{mem}} \approx 5\,\text{s}$. It highlights how the main loss contribution on the short timescales is given by two-body collisions (e.g., the contribution of $\gamma_{1\text{-body}}$ is limited to about 4%). The one-body collisions become, instead, the dominant loss mechanism at long storage times. For instance, for $\tau_{\text{mem}} \approx 100\,\text{s}$, the intrinsic efficiency due to $\gamma_{2\text{-body}}(t)$ is still around 0.90, whereas the collisions with the background gas bring it down to 0.38.

The initial atom density distribution of the BEC determines the expansion rate of the ensemble, which consequently affects the achievable intrinsic memory efficiency, $\eta_1(t) \cdot \eta_2(t)$. Figure 3 shows the trends of the intrinsic memory efficiency for a set of three isotropic BECs with different initial sizes σ_0. All cases have, though, a common initial peak density $\rho_0(0) = 2.3 \times 10^{14}\,\text{cm}^{-3}$ to grant a common initial $\gamma_{2\text{-body}}(0)$. The ensembles expand for 1 s, until collimation, and are then refocused after $T_C = 3\,\text{s}$. The inset displays the trends of the two-body decay rate for the three cases during the initial expansion phase and around the focus. It is evident how, for a common initial peak density, the ensemble expands faster

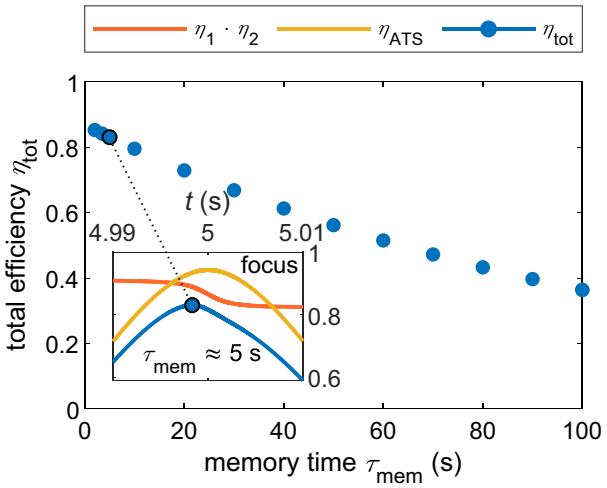

FIG. 4. Calculated overall efficiency as a function of τ_{mem}. For each data point, the readout is performed after refocusing, i.e., at high density. The inset shows a comparison between the overall retrieval efficiency η_{tot}, the efficiency factor η_{ATS}, and the intrinsic memory efficiency $\eta_1 \cdot \eta_2$ as a function of time for $T_C = 3$ s (i.e., $\tau_{mem} \approx 5$ s) during the focus of the BEC.

when it has a smaller initial size, yielding lower accumulated losses from the two-body collisions and therefore granting higher intrinsic efficiencies.

In order to calculate the overall efficiency, η_{tot}, we estimate the optimal write-in and readout efficiency associated with an ATS protocol (in this case in backward retrieval) as [66]

$$\eta_{ATS}(\rho(t)) \approx (1 - e^{-d(t)/(2F)})^2 e^{-1/F}, \tag{6}$$

where $F \approx 2\pi B/\Gamma$ is the "ATS factor" depending on the bandwidth B of the input pulse and the optical transition linewidth Γ; see Appendix C. The effective OD, $d(t)$, results from integration along the probe beam propagation of the spatial overlap between the Thomas-Fermi density distribution of the ensemble and the intensity profile of the probe beam [33]. In this paper, we consider a probe beam with a waist of 1 μm, which is smaller than the radius of the BEC $\sigma(t)$, and a Gaussian temporal profile with full width at half maximum $\tau_p = 2.4$ ns. The pulse bandwidth, $B = 180$ MHz, satisfies the condition for optimal ATS efficiency associated with the condensate OD and the optical linewidth Γ [66].

The total efficiency for a series of on-demand readout cases with different τ_{mem} is calculated through Eq. (3) and presented in Fig. 4. The inset highlights separately the time-dependent contributions to the total memory efficiency η_{tot} (blue line) for the case with 5 s storage time: the ATS efficiency factor η_{ATS} (yellow line) and the intrinsic efficiency $\eta_1 \cdot \eta_2$ (orange line). The write-in and readout efficiency peaks, as expected, when the BEC is focused down to its original size. The maximum in the total efficiency is, however, shifted in time compared with this peak. The enhanced density in the focus indeed leads to a drop in the intrinsic efficiency, as shown in Fig. 2, which in turn consistently causes the peak in the total efficiency to be reached $\delta\tau$ before the focus is achieved. The magnitude of this effect depends on the expansion rate of the BEC: assuming a comparable initial density, a slower expansion of the ensemble generally corresponds to a larger value of $\delta\tau$. Taking into account the three different expansion rates of Fig. 3, we observe $\delta\tau \approx 2$ ms for the case with $\sigma_0 = 3$ μm (blue line), which is also the case presented in Fig. 2; the shift increases to $\delta\tau \approx 5$ ms for $\sigma_0 = 5.1$ μm (orange line); and finally for the case with the slowest expansion corresponding to the initial size $\sigma_0 = 6.5$ μm (yellow line), the shift rises to $\delta\tau \approx 7$ ms. Nevertheless, these shifts remain orders of magnitude lower than the storage times taken into account in this paper.

Each point presented in the main graph of Fig. 4 is, thus, associated with the peak total write-in and readout efficiency after the BEC refocusing. Assuming ideal lensing potentials, overall efficiencies >35% can be reached for τ_{mem} up to 100 s, neglecting external sources of noise. With τ_{mem} of ≈100 s, the proposed memory will thus exhibit an unprecedented time-bandwidth product of $\sim 1 \times 10^{10}$.

V. CONCLUSIONS AND OUTLOOK

In conclusion, by focusing on density-dependent effects on the memory efficiency, we proposed an experimental protocol that extends the storage time of BEC-based quantum memories. This method relies on matter-wave lensing to tune the density of an expanding pure BEC in microgravity. We show storage times that are ultimately limited by the vacuum quality and the consequent collisions with the background gas. Note that aberrations due to anharmonicity of the lensing potentials or possible technical field inhomogeneities are not accounted for in our simulations. Nevertheless, this method can open up the way to push the limit of cold-atom-based quantum memories to $\tau_{mem} \approx 100$ s storage time, which would be of interest for growing demands of long-storage-time memories for space operations [9–13]. We further show that implementing the ATS memory technique in cold-atomic systems has the potential to achieve exceptionally high time-bandwidth products of around 10^{10}, which is an order of magnitude higher than the current state of the art with input-output-type memories [67].

Finally, this protocol that relies on interaction-driven expansion to decrease the atomic density, and consequently the collisional losses, followed by matter-wave optics techniques to collimate and refocus the ensemble, has advantages that are not restricted to the quantum memory field, but can have applications for a broader audience. Proof-of-principle tests of this technique should be readily possible within long-baseline facilities [68–70] and microgravity platforms on the ground, e.g., drop tower facilities [49,71], and ultimately in space [35,36,41].

ACKNOWLEDGMENTS

This work is supported by the German Space Agency (DLR) with funds provided by the BMWK under Grants No. 50WM2055 (OPTIMO-II) and No. 50WM2250B (QUANTUS+). M.G. further acknowledges funding from the European Union's Horizon 2020 research and innovation program under Marie Skłodowska-Curie Grant Agreement No. 894590.

APPENDIX A: SIMULATION OF THE BEC EXPANSION AND REFOCUSING DYNAMICS

Our simulations of an interacting ^{87}Rb BEC follow a scaling approach with Gaussian-shaped trial functions, as described in the main text. From this, a system of coupled evolution equations can be obtained through a variational ansatz [59,60], which contains the nonlinear interaction and the potential for delta kick collimation with time-dependent angular trap frequencies

$$\omega(t) = \begin{cases} \omega, & \text{for } T_0 - \tau_{\mathrm{DKC}}/2 < t < T_0 + \tau_{\mathrm{DKC}}/2 \text{ (collimation)}, \\ \omega, & \text{for } T_0 + T_{\mathrm{C}} - \tau_{\mathrm{DKC}}/2 < t < T_0 + T_{\mathrm{C}} + \tau_{\mathrm{DKC}}/2 \text{ (refocusing)}, \\ 0, & \text{otherwise}, \end{cases} \tag{A1}$$

with T_0, T_{C}, and τ_{DKC} as defined in the main text. The s-wave scattering length is set to $\mathrm{Re}(a_{\mathrm{sc}}) = 100a_0$, where a_0 is the Bohr radius. The evolution of the ensemble's size $\sigma(t)$ and corresponding density distribution $\rho(t)$ of peak density $\rho_0(t)$ are determined during the entire sequence employing the ordinary differential equation (ODE) solver ODE45.

Although we show our results using an isotropic ensemble to enhance the clarity of presentation, it is worth noting that our protocol can be readily applied to the more realistic case of a BEC released from a cigar-shaped trapping potential. Therefore our approach is not restricted to the isotropic case.

The starting sizes σ_0 and atom number N_0 are chosen to set the initial peak densities to a common value of $\rho_0 = 2.3 \times 10^{-14}\,\mathrm{cm}^{-3}$. The initial parameters presented in the figures in the main text are given in Table I.

To put this into the perspective of a realistic experiment, a three-dimensional (3D) numerical simulation based on a split-step Fourier method has been used to find the ground-state wave function of a BEC inside a harmonic release trap [72,73]. We determine the angular trap frequencies ω_0 by matching the standard deviation of the atomic density distribution with the starting size of the scaling approach. The corresponding trap frequencies are included in Table I.

APPENDIX B: DIFFERENTIAL AC-STARK SHIFT

One key feature of the DKC technique is that it relies on inhomogeneous focusing and collimating fields. However, such spatial inhomogeneities might create inhomogeneous broadening of the relevant atomic levels, which, in turn, would create further dephasing. In this Appendix, we quantify the differential AC-Stark shift of the light fields in an all-optical DKC scheme that we present in the main text and show that the inhomogeneous broadening induced by the DKC pulses is sufficiently small that they do not cause any significant dephasing during the pulse duration.

TABLE I. Initial parameters for the scaling approach for the data sets presented in Figs. 2 and 4 in the main text, and in Fig 3 with the corresponding angular trap frequencies of a release trap obtained with a split-step Fourier method.

	σ_0 (μm)	N_0	ρ_0 (cm^{-3})	ω_0 (2π Hz)
Figs. 2 and 4	3.0	1×10^5	2.3×10^{-14}	142
Fig. 3	3.0	1×10^5	2.3×10^{-14}	142
	5.1	5×10^5	2.3×10^{-14}	84
	6.5	1×10^6	2.3×10^{-14}	65

For our optical atom lenses, we consider a harmonic-shaped optical potential

$$V_{\mathrm{DKC}}(r) = -\frac{1}{2}m\omega^2 r^2 = -\frac{1}{2\epsilon_0 c}\mathrm{Re}(\alpha)\cdot I(r) \tag{B1}$$

with atomic polarizability $\alpha_{|i\rangle}(\lambda)$ of the two hyperfine ground states $|g\rangle$ and $|s\rangle$ of ^{87}Rb, representing $|5^2S_{1/2}, F = 1\rangle$ and $|5^2S_{1/2}, F = 2\rangle$, respectively. In the calculation of the atomic polarizability in the presence of the far-red-detuned field of wavelength λ, we only take into account the D_1 and D_2 lines. The inducing light intensity distribution is

$$I(r) = I_0\left(1 - \frac{r^2}{h_0^2}\right)\Theta(h_0 - r), \tag{B2}$$

where I_0 is the peak intensity, $\Theta(x)$ is the Heaviside step function, and h_0 is the characteristic size. We choose the peak intensity depending on h_0 to obtain the desired trap frequency for collimation of the lower-energetic ground state $|g\rangle$

$$\omega = \sqrt{\frac{\alpha_{|g\rangle}(\lambda)I_0}{mc\epsilon_0 h_0^2}} = 2\pi \times 2.25\,\mathrm{Hz}. \tag{B3}$$

The characteristic size of the potential is set to $h_0 = 1\sigma_{\mathrm{max}}$, $2\sigma_{\mathrm{max}}$, and $3\sigma_{\mathrm{max}}$ (which addresses 31.8, 87.0, and 99.2% of the atomic density distribution, respectively), and we calculate the differential AC-Stark shift via

$$\delta\nu_{\mathrm{AC}} = \frac{1}{2\epsilon_0 c}\frac{I_0}{h}|\alpha_{|s\rangle}(\lambda) - \alpha_{|g\rangle}(\lambda)|. \tag{B4}$$

Figure 5 illustrates the spatial distribution of the differential AC-Stark shift for variously sized potentials, with the corresponding light intensities and trap frequencies, in comparison with the atomic density distribution during the DKC pulses (as shown in Fig. 2 in the main text). The maximum differential AC-Stark shift experienced by the atomic ensemble has been calculated for potentials of different characteristic sizes and wavelengths, as recorded in Table II, and we verify that the decoherence caused by the DKC pulses for the case presented in the main text ($\tau_{\mathrm{DKC}} = 5\,\mathrm{ms}$ and $\lambda = 1064\,\mathrm{nm}$) is negligible.

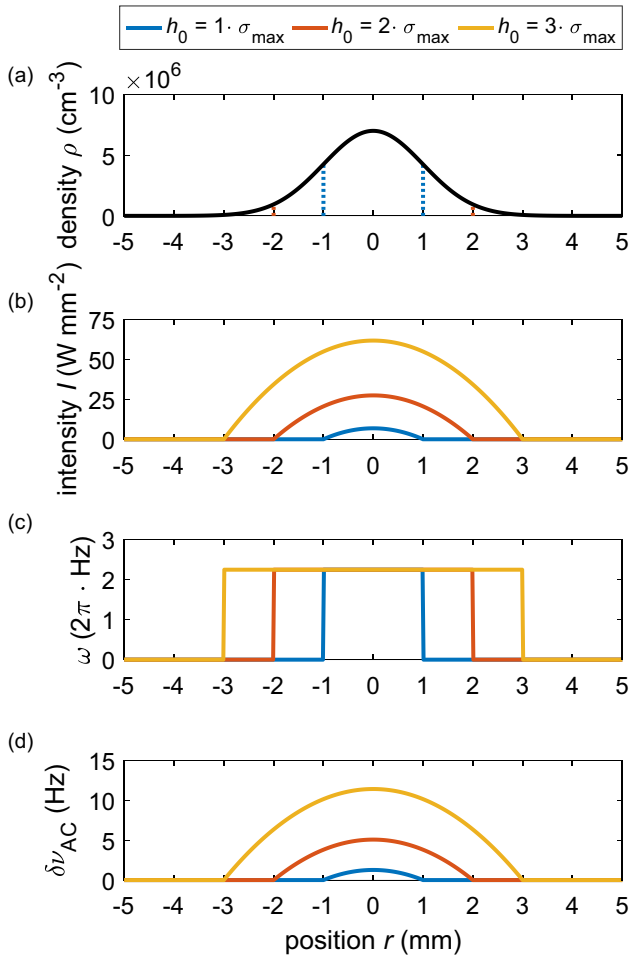

FIG. 5. Comparison of (a) the atomic density distribution during the DKC pulses (presented in Fig. 2 in the main text); (b) the optical intensity distribution needed for a harmonic-shaped DKC potential of (c) trap frequencies leading to (d) differential AC-Stark shifts between the two hyperfine ground states for different characteristic sizes h_0.

APPENDIX C: MEMORY EFFICIENCY WITH THE AUTLER-TOWNES SPLITTING PROTOCOL

The intrinsic memory efficiency calculations that are presented in the main text are independent of the specific memory protocol. On the other hand, write-in and readout efficiencies depend on the specific protocol, which may have different behaviors with respect to ODs and noise. We decided to incorporate the recently demonstrated Autler-Townes splitting (ATS) protocol [33,57] into our work due to its favorable dependence on the OD and its low-noise characteristics. In this Appendix, we discuss the main features of the ATS protocol concerning bandwidth and efficiency, their connections with each other, and the related OD calculations. We will follow the treatment in Ref. [33] while doing so.

TABLE II. Parameters of optical potentials for DKC and the associated maximum differential AC-Stark shift experienced by the atomic ensemble. We added the AC-Stark shifts associated with two additional wavelengths for comparison.

λ (nm)	h_0 (mm)	ω (2π Hz)	I_0 (W mm^{-2})	$\delta\nu_{AC}$ (Hz)
1064	1.0	2.25	6.85	1.27
1064	2.0	2.25	27.42	5.06
1064	3.0	2.25	61.70	11.39
1000	3.0	2.25	51.93	14.40
900	3.0	2.25	32.26	25.86

1. Optimal ATS efficiency in the backward retrieval configuration

Throughout the main text, we assume backward retrieval of the probe signal, using counterpropagating write-in and readout control pulses. In this configuration, the readout dynamics are a time reverse of the ones occurring during the storage procedure. This configuration allows us to reduce the influence of the reabsorption of the retrieved pulses by the atomic medium, which sets a limit on the maximum efficiency achievable in the forward configuration [74,75].

The ATS efficiency in the backward configuration is [33]

$$\eta_{\mathrm{ATS\,back}}(\rho) \approx (1 - e^{-d/(2F)})^2 e^{-1/F}, \tag{C1}$$

where d is the effective peak optical depth and $F = 2\pi B/\Gamma$ is the "ATS factor" associated with the bandwidth of the probe pulse B and the atomic transition linewidth Γ. In the main text, we consider the D_1 line of ^{87}Rb; thus $\Gamma = 2\pi \times 5.7500(56)$ MHz [76]. We assume input pulses with a Gaussian temporal profile, defined by a full width at half maximum τ_p. The associated bandwidth for a Gaussian profile is $B = (2\ln(2)/2)/\tau_p$. Equation (C1) is maximized for bandwidths that are large compared with the atomic transition and for optical depths which satisfy $d/(2F) \geqslant 4$ [33,66]. All the efficiencies presented in Fig. 4 in the main text are inferred for $B = 180$ MHz, corresponding to the optimal bandwidth for the peak optical depths taken into account in the calculations.

2. Effective optical depth

The effective optical depth of an atomic ensemble for probe intensity far below the atom's saturation intensity can be derived from Beer's law as

$$d = -\ln\left(\frac{\iint \mathrm{I_{out}}(x,y)\,dx\,dy}{\iint \mathrm{I_{in}}(x,y)\,dx\,dy}\right), \tag{C2}$$

where $\mathrm{I_{in}}(x,y)$ [$\mathrm{I_{out}}(x,y)$] represents the intensity distribution of the input (output) beam propagating along the z direction through the atomic ensemble. In our case, we assume as input intensity a Gaussian beam profile, described by a peak intensity $\mathrm{I_0}$ and beam radius w as

$$\mathrm{I_{in}}(x,y) = \mathrm{I_0}\exp\left(-2\frac{x^2+y^2}{w^2}\right), \tag{C3}$$

which leads to an output profile of the form

$$\mathrm{I_{out}}(x,y) = \mathrm{I_{in}}(x,y)\exp\left[-d_0(x,y)\right], \tag{C4}$$

with the resonant optical depth profile expressed as

$$d_0(x,y) = \sigma_0 \int_0^L \rho(x,y,z)\,dz = \sigma_0 \rho^{2\mathrm{D}}(x,y), \tag{C5}$$

where σ_0 is the resonant atom-photon scattering cross section associated with the transition, while the second term, $\rho^{2D}(x, y)$, represents the line-integrated atomic density distribution.

For a BEC, the atomic density is defined by a Thomas-Fermi profile, expressed as

$$\rho^{TF}(x, y) = \frac{\mu}{g}\left(1 - \frac{x^2}{R_x^2} - \frac{y^2}{R_y^2} - \frac{z^2}{R_z^2}\right), \tag{C6}$$

where the peak density of the condensate is given by μ/g, with μ representing the chemical potential and $g = 4\pi\hbar^2 \mathrm{Re}(a_{sc})/m$ representing the interaction parameter dependent on the s-wave scattering length a_{sc}. Considering an isotropic atomic ensemble, as in this paper, the Thomas-Fermi radii are the same, $R_x = R_y = R_z = R$, yielding a line-integrated atomic density

$$\rho^{2D}(x, y) = \frac{4R}{3}\frac{\mu}{g}\left(1 - \frac{x^2 + y^2}{R^2}\right)^{3/2}. \tag{C7}$$

Substituting Eq. (C7) into Eq. (C5), it is possible to obtain the resonant optical depth d_0, which depends only on the properties of the atomic ensemble. This needs to be inserted within Eq. (C2) to obtain the effective optical depth d, which takes into account the properties of the probing beam. It should be mentioned that, as the Rayleigh length is comparable to the size of the ensemble, we assume a constant size of the beam in the integration. The highest $d \approx d_0$, and therefore the highest memory efficiency, is reached when the probe beam is focused on the region of the peak atomic density with a size that is much smaller than the condensate.

[1] N. Sangouard, C. Simon, H. de Riedmatten, and N. Gisin, Quantum repeaters based on atomic ensembles and linear optics, Rev. Mod. Phys. **83**, 33 (2011).

[2] K. Heshami, D. G. England, P. C. Humphreys, P. J. Bustard, V. M. Acosta, J. Nunn, and B. J. Sussman, Quantum memories: Emerging applications and recent advances, J. Mod. Opt. **63**, 2005 (2016).

[3] J. Nunn, N. K. Langford, W. S. Kolthammer, T. F. M. Champion, M. R. Sprague, P. S. Michelberger, X.-M. Jin, D. G. England, and I. A. Walmsley, Enhancing Multiphoton Rates with Quantum Memories, Phys. Rev. Lett. **110**, 133601 (2013).

[4] E. Gouzien and N. Sangouard, Factoring 2048-bit RSA Integers in 177 Days with 13436 Qubits and a Multimode Memory, Phys. Rev. Lett. **127**, 140503 (2021).

[5] M. Gündoğan, J. S. Sidhu, V. Henderson, L. Mazzarella, J. Wolters, D. K. L. Oi, and M. Krutzik, Proposal for space-borne quantum memories for global quantum networking, npj Quantum Inf. **7**, 128 (2021).

[6] C. Liorni, H. Kampermann, and D. Bruß, Quantum repeaters in space, New J. Phys. **23**, 053021 (2021).

[7] J. S. Sidhu, S. K. Joshi, M. Gündoğan, T. Brougham, D. Lowndes, L. Mazzarella, M. Krutzik, S. Mohapatra, D. Dequal, G. Vallone, P. Villoresi, A. Ling, T. Jennewein, M. Mohageg, J. G. Rarity, I. Fuentes, S. Pirandola, and D. K. L. Oi, Advances in space quantum communications, IET Quantum Commun. **2**, 182 (2021).

[8] J. Wallnöfer, F. Hahn, M. Gündoğan, J. S. Sidhu, F. Wiesner, N. Walk, J. Eisert, and J. Wolters, Simulating quantum repeater strategies for multiple satellites, Commun. Phys. **5**, 169 (2022).

[9] Y. Cao, Y.-H. Li, W.-J. Zou, Z.-P. Li, Q. Shen, S.-K. Liao, J.-G. Ren, J. Yin, Y.-A. Chen, C.-Z. Peng, and J.-W. Pan, Bell Test over Extremely High-Loss Channels: Towards Distributing Entangled Photon Pairs between Earth and the Moon, Phys. Rev. Lett. **120**, 140405 (2018).

[10] M. Mohageg, L. Mazzarella, D. V. Strekalov, N. Yu, A. Zhai, S. Johnson, C. Anastopoulos, J. Gallicchio, B. L. Hu, T. Jennewein, S.-Y. Lin, A. Ling, C. Marquardt, M. Meister, A. Roura, L. Wörner, N. Yu, A. Zhai, and P. Kwiat, The deep space quantum link: Prospective fundamental physics experiments using long-baseline quantum optics, EPJ Quantum Technol. **9**, 25 (2022).

[11] M. Gündoğan, T. Jennewein, F. K. Asadi, E. D. Ros, E. Sağlamyürek, D. Oblak, T. Vogl, D. Rieländer, J. Sidhu, S. Grandi, L. Mazzarella, J. Wallnöfer, P. Ledingham, L. LeBlanc, M. Mazzera, M. Mohageg, J. Wolters, A. Ling, M. Atatüre, H. de Riedmatten *et al.*, Topical white paper: A case for quantum memories in space, arXiv:2111.09595.

[12] C.-Y. Lu, Y. Cao, C.-Z. Peng, and J.-W. Pan, Micius quantum experiments in space, Rev. Mod. Phys. **94**, 035001 (2022).

[13] R. Barzel, M. Gündoğan, M. Krutzik, D. Rätzel, and C. Lämmerzahl, Gravitationally induced entanglement dynamics of photon pairs and quantum memories, arXiv:2209.02099.

[14] G. D. Fuchs, G. Burkard, P. V. Klimov, and D. D. Awschalom, A quantum memory intrinsic to single nitrogen–vacancy centres in diamond, Nat. Phys. **7**, 789 (2011).

[15] D. D. Sukachev, A. Sipahigil, C. T. Nguyen, M. K. Bhaskar, R. E. Evans, F. Jelezko, and M. D. Lukin, Silicon-Vacancy Spin Qubit in Diamond: A Quantum Memory Exceeding 10 ms with Single-Shot State Readout, Phys. Rev. Lett. **119**, 223602 (2017).

[16] C. E. Bradley, J. Randall, M. H. Abobeih, R. C. Berrevoets, M. J. Degen, M. A. Bakker, M. Markham, D. J. Twitchen, and T. H. Taminiau, A Ten-Qubit Solid-State Spin Register with Quantum Memory up to One Minute, Phys. Rev. X **9**, 031045 (2019).

[17] P. M. Ledingham, W. R. Naylor, and J. J. Longdell, Experimental Realization of Light with Time-Separated Correlations by Rephasing Amplified Spontaneous Emission, Phys. Rev. Lett. **109**, 093602 (2012).

[18] P. Jobez, C. Laplane, N. Timoney, N. Gisin, A. Ferrier, P. Goldner, and M. Afzelius, Coherent Spin Control at the Quantum Level in an Ensemble-Based Optical Memory, Phys. Rev. Lett. **114**, 230502 (2015).

[19] M. Gündoğan, P. M. Ledingham, K. Kutluer, M. Mazzera, and H. de Riedmatten, Solid State Spin-Wave Quantum Memory for Time-Bin Qubits, Phys. Rev. Lett. **114**, 230501 (2015).

[20] C. Langer, R. Ozeri, J. D. Jost, J. Chiaverini, B. DeMarco, A. Ben-Kish, R. B. Blakestad, J. Britton, D. B. Hume, W. M. Itano, D. Leibfried, R. Reichle, T. Rosenband, T. Schaetz, P. O. Schmidt, and D. J. Wineland, Long-Lived Qubit Memory Using Atomic Ions, Phys. Rev. Lett. **95**, 060502 (2005).

[21] T. P. Harty, D. T. C. Allcock, C. J. Ballance, L. Guidoni, H. A. Janacek, N. M. Linke, D. N. Stacey, and D. M. Lucas, High-Fidelity Preparation, Gates, Memory, and Readout of a Trapped-Ion Quantum Bit, Phys. Rev. Lett. **113**, 220501 (2014).

[22] P. Wang, C.-Y. Luan, M. Qiao, M. Um, J. Zhang, Y. Wang, X. Yuan, M. Gu, J. Zhang, and K. Kim, Single ion qubit with estimated coherence time exceeding one hour, Nat. Commun. **12**, 233 (2021).

[23] H. P. Specht, C. Nölleke, A. Reiserer, M. Uphoff, E. Figueroa, S. Ritter, and G. Rempe, A single-atom quantum memory, Nature (London) **473**, 190 (2011).

[24] S. Langenfeld, P. Thomas, O. Morin, and G. Rempe, Quantum Repeater Node Demonstrating Unconditionally Secure Key Distribution, Phys. Rev. Lett. **126**, 230506 (2021).

[25] Y.-W. Cho, G. T. Campbell, J. L. Everett, J. Bernu, D. B. Higginbottom, M. T. Cao, J. Geng, N. P. Robins, P. K. Lam, and B. C. Buchler, Highly efficient optical quantum memory with long coherence time in cold atoms, Optica **3**, 100 (2016).

[26] J. Wolters, G. Buser, A. Horsley, L. Béguin, A. Jöckel, J.-P. Jahn, R. J. Warburton, and P. Treutlein, Simple Atomic Quantum Memory Suitable for Semiconductor Quantum Dot Single Photons, Phys. Rev. Lett. **119**, 060502 (2017).

[27] O. Katz and O. Firstenberg, Light storage for one second in room-temperature alkali vapor, Nat. Commun. **9**, 2074 (2018).

[28] K. T. Kaczmarek, P. M. Ledingham, B. Brecht, S. E. Thomas, G. S. Thekkadath, O. Lazo-Arjona, J. H. D. Munns, E. Poem, A. Feizpour, D. J. Saunders, J. Nunn, and I. A. Walmsley, High-speed noise-free optical quantum memory, Phys. Rev. A **97**, 042316 (2018).

[29] S. Riedl, M. Lettner, C. Vo, S. Baur, G. Rempe, and S. Dürr, Bose-einstein condensate as a quantum memory for a photonic polarization qubit, Phys. Rev. A **85**, 022318 (2012).

[30] Y. Wang, J. Li, S. Zhang, K. Su, Y. Zhou, K. Liao, S. Du, H. Yan, and S.-L. Zhu, Efficient quantum memory for single-photon polarization qubits, Nat. Photonics **13**, 346 (2019).

[31] X.-H. Bao, A. Reingruber, P. Dietrich, J. Rui, A. Dück, T. Strassel, L. Li, N.-L. Liu, B. Zhao, and J.-W. Pan, Efficient and long-lived quantum memory with cold atoms inside a ring cavity, Nat. Phys. **8**, 517 (2012).

[32] L. Heller, P. Farrera, G. Heinze, and H. de Riedmatten, Cold-Atom Temporally Multiplexed Quantum Memory with Cavity-Enhanced Noise Suppression, Phys. Rev. Lett. **124**, 210504 (2020).

[33] E. Saglamyurek, T. Hrushevskyi, A. Rastogi, L. W. Cooke, B. D. Smith, and L. J. LeBlanc, Storing short single-photon-level optical pulses in Bose–Einstein condensates for high-performance quantum memory, New J. Phys. **23**, 043028 (2021).

[34] L. Liu, D.-S. Lü, W.-B. Chen, T. Li, Q.-Z. Qu, B. Wang, L. Li, W. Ren, Z.-R. Dong, J.-B. Zhao, W.-B. Xia, X. Zhao, J.-W. Ji, M.-F. Ye, Y.-G. Sun, Y.-Y. Yao, D. Song, Z.-G. Liang, S.-J. Hu, D.-H. Yu *et al.*, In-orbit operation of an atomic clock based on laser-cooled ^{87}Rb atoms, Nat. Commun. **9**, 2760 (2018).

[35] D. Becker, M. D. Lachmann, S. T. Seidel, H. Ahlers, A. N. Dinkelaker, J. Grosse, O. Hellmig, H. Müntinga, V. Schkolnik, T. Wendrich, A. Wenzlawski, B. Weps, R. Corgier, T. Franz, N. Gaaloul, W. Herr, D. Lüdtke, M. Popp, S. Amri, H. Duncker *et al.*, Space-borne Bose-Einstein condensation for precision interferometry, Nature (London) **562**, 391 (2018).

[36] D. C. Aveline, J. R. Williams, E. R. Elliott, C. Dutenhoffer, J. R. Kellogg, J. M. Kohel, N. E. Lay, K. Oudrhiri, R. F. Shotwell, N. Yu, and R. J. Thompson, Observation of Bose–Einstein condensates in an Earth-orbiting research lab, Nature (London) **582**, 193 (2020).

[37] I. Alonso, C. Alpigiani, B. Altschul, H. Araujo, G. Arduini, J. Arlt, L. Badurina, A. Balaz, S. Bandarupally, B. C. B. M. Barone, M. Barsanti, S. Bass, A. Bassi, B. Battelier, C. F. A. Baynham, Q. Beaufils, A. Belić, J. Bergé, J. Bernabeu, A. Bertoldi *et al.*, Cold atoms in space: Community workshop summary and proposed road-map, EPJ Quantum Technol. **9**, 30 (2022).

[38] G. M. Tino, A. Bassi, G. Bianco, K. Bongs, P. Bouyer, L. Cacciapuoti, S. Capozziello, X. Chen, M. L. Chiofalo, A. Derevianko, W. Ertmer, N. Gaaloul, P. Gill, P. W. Graham, J. M. Hogan, L. Iess, M. A. Kasevich, H. Katori, C. Klempt, X. Lu *et al.*, SAGE: A proposal for a space atomic gravity explorer, Eur. Phys. J. D **73**, 228 (2019).

[39] Y. A. El-Neaj, C. Alpigiani, S. Amairi-Pyka, H. Araújo, A. Balaž, A. Bassi, L. Bathe-Peters, B. Battelier, A. Belić, E. Bentine, J. Bernabeu, A. Bertoldi, R. Bingham, D. Blas, V. Bolpasi, K. Bongs, S. Bose, P. Bouyer, T. Bowcock, W. Bowden *et al.*, AEDGE: Atomic experiment for dark matter and gravity exploration in space, EPJ Quantum Technology **7**, 6 (2020).

[40] L. Cacciapuoti, M. Armano, R. Much, O. Sy, A. Helm, M. P. Hess, J. Kehrer, S. Koller, T. Niedermaier, F. X. Esnault, D. Massonnet, D. Goujon, J. Pittet, P. Rochat, S. Liu, W. Schaefer, T. Schwall, I. Prochazka, A. Schlicht, U. Schreiber *et al.*, Testing gravity with cold-atom clocks in space, Eur. Phys. J. D **74**, 164 (2020).

[41] K. Frye, S. Abend, W. Bartosch, A. Bawamia, D. Becker, H. Blume, C. Braxmaier, S.-W. Chiow, M. A. Efremov, W. Ertmer, P. Fierlinger, T. Franz, N. Gaaloul, J. Grosse, C. Grzeschik, O. Hellmig, V. A. Henderson, W. Herr, U. Israelsson, J. Kohel *et al.*, The Bose-Einstein condensate and cold atom laboratory, EPJ Quantum Technol. **8**, 1 (2021).

[42] Y. O. Dudin, L. Li, and A. Kuzmich, Light storage on the time scale of a minute, Phys. Rev. A **87**, 031801(R) (2013).

[43] N. Lundblad, M. Schlosser, and J. V. Porto, Experimental observation of magic-wavelength behavior of ^{87}Rb atoms in an optical lattice, Phys. Rev. A **81**, 031611(R) (2010).

[44] Y. O. Dudin, R. Zhao, T. A. B. Kennedy, and A. Kuzmich, Light storage in a magnetically dressed optical lattice, Phys. Rev. A **81**, 041805(R) (2010).

[45] R. Zhang, S. R. Garner, and L. V. Hau, Creation of Long-Term Coherent Optical Memory via Controlled Nonlinear Interactions in Bose-Einstein Condensates, Phys. Rev. Lett. **103**, 233602 (2009).

[46] H. Ammann and N. Christensen, Delta Kick Cooling: A New Method for Cooling Atoms, Phys. Rev. Lett. **78**, 2088 (1997).

[47] S. H. Myrskog, J. K. Fox, H. S. Moon, J. B. Kim, and A. M. Steinberg, Modified "δ-kick cooling" using magnetic field gradients, Phys. Rev. A **61**, 053412 (2000).

[48] T. Kovachy, J. M. Hogan, A. Sugarbaker, S. M. Dickerson, C. A. Donnelly, C. Overstreet, and M. A. Kasevich, Matter Wave Lensing to Picokelvin Temperatures, Phys. Rev. Lett. **114**, 143004 (2015).

[49] C. Deppner, W. Herr, M. Cornelius, P. Stromberger, T. Sternke, C. Grzeschik, A. Grote, J. Rudolph, S. Herrmann, M. Krutzik, A. Wenzlawski, R. Corgier, E. Charron, D. Guéry-Odelin, N.

Gaaloul, C. Lämmerzahl, A. Peters, P. Windpassinger, and E. M. Rasel, Collective-Mode Enhanced Matter-Wave Optics, Phys. Rev. Lett. **127**, 100401 (2021).

[50] J. M. Hogan, D. M. S. Johnson, S. Dickerson, T. Kovachy, A. Sugarbaker, S.-w. Chiow, P. W. Graham, M. A. Kasevich, B. Saif, S. Rajendran, P. Bouyer, B. D. Seery, L. Feinberg, and R. Keski-Kuha, An atomic gravitational wave interferometric sensor in low earth orbit (AGIS-LEO), Gen. Relativ. Gravitation **43**, 1953 (2011).

[51] T. Nirrengarten, A. Qarry, C. Roux, A. Emmert, G. Nogues, M. Brune, J.-M. Raimond, and S. Haroche, Realization of a Superconducting Atom Chip, Phys. Rev. Lett. **97**, 200405 (2006).

[52] T. Luan, Y. Li, X. Zhang, and X. Chen, Realization of two-stage crossed beam cooling and the comparison with delta-kick cooling in experiment, Rev. Sci. Instrum. **89**, 123110 (2018).

[53] S. Kanthak, M. Gebbe, M. Gersemann, S. Abend, E. M. Rasel, and M. Krutzik, Time-domain optics for atomic quantum matter, New J. Phys. **23**, 093002 (2021).

[54] D. Gochnauer, T. Rahman, A. Wirth-Singh, and S. Gupta, Interferometry in an atomic fountain with ytterbium Bose-Einstein condensates, Atoms **9**, 58 (2021).

[55] M. Namazi, G. Vallone, B. Jordaan, C. Goham, R. Shahrokhshahi, P. Villoresi, and E. Figueroa, Free-Space Quantum Communication with a Portable Quantum Memory, Phys. Rev. Appl. **8**, 064013 (2017).

[56] A. V. Gorshkov, A. André, M. Fleischhauer, A. S. Sørensen, and M. D. Lukin, Universal Approach to Optimal Photon Storage in Atomic Media, Phys. Rev. Lett. **98**, 123601 (2007).

[57] E. Saglamyurek, T. Hrushevskyi, A. Rastogi, K. Heshami, and L. J. LeBlanc, Coherent storage and manipulation of broadband photons via dynamically controlled Autler–Townes splitting, Nat. Photonics **12**, 774 (2018).

[58] J. Geng, G. T. Campbell, J. Bernu, D. B. Higginbottom, B. M. Sparkes, S. M. Assad, W. P. Zhang, N. P. Robins, P. K. Lam, and B. C. Buchler, Electromagnetically induced transparency and four-wave mixing in a cold atomic ensemble with large optical depth, New J. Phys. **16**, 113053 (2014).

[59] V. M. Pérez-García, H. Michinel, J. I. Cirac, M. Lewenstein, and P. Zoller, Dynamics of Bose-Einstein condensates: Variational solutions of the Gross-Pitaevskii equations, Phys. Rev. A **56**, 1424 (1997).

[60] V. M. Pérez-García, H. Michinel, J. I. Cirac, M. Lewenstein, and P. Zoller, Low Energy Excitations of a Bose-Einstein Condensate: A Time-Dependent Variational Analysis, Phys. Rev. Lett. **77**, 5320 (1996).

[61] D. M. Harber, H. J. Lewandowski, J. M. McGuirk, and E. A. Cornell, Effect of cold collisions on spin coherence and resonance shifts in a magnetically trapped ultracold gas, Phys. Rev. A **66**, 053616 (2002).

[62] R. Corgier, S. Loriani, H. Ahlers, K. Posso-Trujillo, C. Schubert, E. M. Rasel, E. Charron, and N. Gaaloul, Interacting quantum mixtures for precision atom interferometry, New J. Phys. **22**, 123008 (2020).

[63] H. Albers, R. Corgier, A. Herbst, A. Rajagopalan, C. Schubert, C. Vogt, M. Woltmann, C. Lämmerzahl, S. Herrmann, E. Charron, W. Ertmer, E. M. Rasel, N. Gaaloul, and D. Schlippert, All-optical matter-wave lens using time-averaged potentials, Commun. Phys. **5**, 60 (2022).

[64] E. A. Burt, R. W. Ghrist, C. J. Myatt, M. J. Holland, E. A. Cornell, and C. E. Wieman, Coherence, Correlations, and Collisions: What One Learns about Bose-Einstein Condensates from Their Decay, Phys. Rev. Lett. **79**, 337 (1997).

[65] M. Egorov, Coherence and collective oscillations of a two-component Bose-Einstein condensate, Ph.D. thesis, Swinburne University of Technology, 2012.

[66] A. Rastogi, E. Saglamyurek, T. Hrushevskyi, S. Hubele, and L. J. LeBlanc, Discerning quantum memories based on electromagnetically-induced-transparency and Autler-Townes-splitting protocols, Phys. Rev. A **100**, 012314 (2019).

[67] Y. Ma, Y.-Z. Ma, Z.-Q. Zhou, C.-F. Li, and G.-C. Guo, One-hour coherent optical storage in an atomic frequency comb memory, Nat. Commun. **12**, 2381 (2021).

[68] K. S. Hardman, P. J. Everitt, G. D. McDonald, P. Manju, P. B. Wigley, M. A. Sooriyabandara, C. C. N. Kuhn, J. E. Debs, J. D. Close, and N. P. Robins, Simultaneous Precision Gravimetry and Magnetic Gradiometry with a Bose-Einstein Condensate: A High Precision, Quantum Sensor, Phys. Rev. Lett. **117**, 138501 (2016).

[69] P. Asenbaum, C. Overstreet, T. Kovachy, D. D. Brown, J. M. Hogan, and M. A. Kasevich, Phase Shift in an Atom Interferometer due to Spacetime Curvature across its Wave Function, Phys. Rev. Lett. **118**, 183602 (2017).

[70] E. Wodey, D. Tell, E. M. Rasel, D. Schlippert, R. Baur, U. Kissling, B. Kölliker, M. Lorenz, M. Marrer, U. Schläpfer, M. Widmer, C. Ufrecht, S. Stuiber, and P. Fierlinger, A scalable high-performance magnetic shield for very long baseline atom interferometry, Rev. Sci. Instrum. **91**, 035117 (2020).

[71] H. Müntinga, H. Ahlers, M. Krutzik, A. Wenzlawski, S. Arnold, D. Becker, K. Bongs, H. Dittus, H. Duncker, N. Gaaloul, C. Gherasim, E. Giese, C. Grzeschik, T. W. Hänsch, O. Hellmig, W. Herr, S. Herrmann, E. Kajari, S. Kleinert, C. Lämmerzahl *et al.*, Interferometry with Bose-Einstein Condensates in Microgravity, Phys. Rev. Lett. **110**, 093602 (2013).

[72] S. Vowe, pytalises, https://github.com/savowe/pytalises, version v0.2.7, last revised 20 November 2020.

[73] A. Goldberg and J. L. Schwartz, Integration of the Schrödinger equation in imaginary time, J. Comput. Phys. **1**, 433 (1967).

[74] N. Sangouard, C. Simon, J. Minář, H. Zbinden, H. de Riedmatten, and N. Gisin, Long-distance entanglement distribution with single-photon sources, Phys. Rev. A **76**, 050301(R) (2007).

[75] M. Afzelius, C. Simon, H. de Riedmatten, and N. Gisin, Multimode quantum memory based on atomic frequency combs, Phys. Rev. A **79**, 052329 (2009).

[76] D. Steck, Rubidium 87 D line data, https://steck.us/alkalidata, version 2.2.2, last revised 9 July 2021.